DETERMINISTIC METHODS OF SOUND-FIELD COMPUTATION

by

C.W. Spofford and H.M. Garon
Acoustic Environmental Support Detachment
Office of Naval Research
Arlington, Virginia 22217
U.S.A.

ABSTRACT

Models for acoustic propagation in the ocean environment have matured to a level where they are used routinely to estimate deterministic phenomena and, most recently, have been applied to the investigation of stochastic phenomena. This paper reviews the capabilities and limitations of the state-of-the-art acoustic models in the deterministic domain to assist in their fruitful applications to stochastic problems. Formulations based upon ray and wave (both normal-mode and parabolic-equation) techniques are developed from the acoustic wave equation to their most advanced forms. The applicability of these techniques to classes of stochastic phenomena is also discussed.

INTRODUCTION

The results of a series of carefully planned and executed acoustic-oceanographic measurements in the past several years have clearly demonstrated that the ocean has sufficient stability to permit the prediction of a number of acoustic phenomena by models based upon the deterministic (and in this case time-independent) acoustic wave equation. Given that the acoustic wave equation describes the significant features of propagation, the investigation of a particular phenomenon devolves to the questions of environmental inputs and solution techniques. This paper is concerned primarily with the second question: given a complete, deterministic description of the ocean environment, how does one evaluate the acoustic field?

The first portion of the discussion reviews the development of the three types of deterministic solutions currently in use: ray techniques, normal-mode approaches, and the parabolic-equation method. Solutions based upon the three techniques are compared to illustrate the accuracies of the various approximations. The environment is discussed only to the extent that it influences the formulations of a number of approaches. (For example, the continuity of the sound-speed profile is an environmental consideration which has consumed a disproportionate amount of the acoustic-modeler's attention in the ray-tracing treatments.)

Each of the techniques has certain strengths and limitations within the context of deterministic problems, but their applicability to stochastic problems introduces a number of new considerations. There has been an unfortunate tendency, paraphrasing J. B. Keller, to apply models already discredited in the deterministic domain to the solution of stochastic problems. The rush to carry the formulation of the stochastic problem as far as possible before implementation on the computer should not be so all-consuming that the underlying deterministic problem is poorly solved. The final section of this paper addresses some of the practical as well as fundamental limitations of these basic techniques when applied to study stochastic effects.

I. MATHEMATICAL DEVELOPMENT OF THE SOLUTIONS

The propagation of sound in the sea is described mathematically by solutions to the wave equation. Given a monochromatic source of angular frequency ω, at position $\underline{x}'$ in a medium with refractive index $n(\underline{x})$ $(=c_o/c(\underline{x})$, c_o a reference sound speed), then the acoustic pressure $P(\underline{x})$ is obtained from

$$\left[\nabla^2+k^2n^2(\underline{x})\right] P(\underline{x}) = -4\pi\delta(\underline{x}-\underline{x}'), \qquad (1)$$

where the wavenumber $k = \omega/c_o$.

The exact solution of this elliptic partial differential equation, even with boundary conditions at finite range and depth vice the more appropriate radiation conditions, would require an unacceptably lengthy iterative solution on a mesh of impractical size even for today's large digital computers. As an alternative, solutions have been developed which are either approximate (ray and parabolic equation) or exact for more restricted problems (normal modes).

The ray solutions correspond to a high-frequency or large k approximation which, with certain frequency-dependent extensions, may be applicable in deep-water cases for frequencies as low as 25 Hz. Normal-mode solutions, while exact in the range-independent geometry, are practical only for the lower frequencies (less than a few hundred hertz, again in deep water). The parabolic equation solution is also practical only for low frequencies, however

it does permit range variations in the environment so long as no paths of interest are propagating at steep angles (~20 degrees measured from the horizontal). The following sections describe the derivations of these solutions.

In underwater-sound applications, results are typically expressed in terms of intensity and transmission loss rather than pressure. The intensity for a time-harmonic source and locally plane waves is simply

$$I(\underline{x}) = \frac{P^*P}{\rho(\underline{x})\,c(\underline{x})}, \tag{2}$$

where ρ is the density and c the sound speed. Intensities are usually referenced to the intensity, I_o, at a unit distance of 1 yard, hence for a constant-density medium (reasonable within the water column)

$$\frac{I(\underline{x})}{I_o} = \frac{P^*P}{c(\underline{x})} \cdot \frac{c(\underline{x}')}{P_o^*P_o} \quad . \tag{3}$$

Finally, transmission loss relative to one yard is defined as

$$TL = 10\ \mathrm{Log}_{10}\left(\frac{I}{I_o}\right) \tag{4}$$

and in numerical caluclations the intensity at unit distance is taken to be 1.

A. Ray Theory

Ray acoustics traditionally begins with the "ansatz" or postulated solution that the acoustic field may be written as a discrete sum of quasi-plane waves,

$$P(\underline{x},\underline{x}') = \sum_j A_j(\underline{x},\underline{x}') e^{ik\phi_j(\underline{x},\underline{x}')} . \tag{5}$$

When this trial solution is inserted into the wave equation and only the lowest order terms in k are retained, one obtains the eikonal equation

$$\left[\nabla\phi_j(\underline{x},\underline{x}')\right]^2 = n^2(\underline{x}) \tag{6a}$$

and the transport equation

$$\nabla\cdot\left[A_j(\underline{x},\underline{x}')\nabla\phi_j(\underline{x},\underline{x}')\right] = 0. \tag{6b}$$

The eikonal equation in turn yields a set of differential equations describing the ray trajectories, while the transport equation, requiring energy to be conserved along the ray tube, provides the ray amplitudes.

For example, within media which are cylindrically symmetric about the source, the rays may be represented as propagating in a vertical plane and the intensity ratio of equation (3) may be defined as

$$\frac{I}{I_o} = \left(\frac{\cos\theta'}{x}\right)\left(\frac{1}{\sin\theta\left[\frac{\partial x}{\partial\theta'}\right]_z}\right), \qquad (7)$$

where x is the horizontal range ($x'=0$), z the depth of the field point, and the angles θ and θ' correspond to the ray angles measured with respect to the horizontal at the field point and source, respectively. The first term of equation (7) may then be interpreted as the ray-tube's azimuthal divergence and the second as its vertical divergence.

An alternative ansatz to equation (5) begins with the solution written in terms of a continuous superposition of quasi-plane waves [1],

$$P(\underline{x}) = e^{-i\pi/4}\left(\frac{k}{2\pi}\right)^{1/2}\int_{-\infty}^{+\infty} g(\underline{x},\xi)e^{ikf(\underline{x},\xi)}d\xi, \qquad (8)$$

where g and f are determined by the local geometry and the medium. Evaluated asymptotically, the integral is dominated by contributions to the integrand near the points of "stationary phase", ξ_j, which satisfy

$$\frac{\partial}{\partial\xi}f(\underline{x},\xi_j) = 0 \ . \qquad (9)$$

When these points are well-separated from each other and any singularities in $g(\underline{x},\xi)$, the formulation in equation (5) is obtained, where now

$$A_j(\underline{x}) = g(\underline{x},\xi_j) \Big/ \left(f_{\xi\xi}(\underline{x},\xi_j)\right)^{1/2} \qquad (10)$$

and

$$\phi_j(\underline{x}) = f(\underline{x},\xi_j) \ . \qquad (11)$$

These points of stationary phase then correspond to the ray paths connecting the points $\underline{x}$ and $\underline{x}'$. The phases ϕ_j correspond to the travel times along these rays plus any descrete phase shifts acquired by the rays (e.g. $-\pi$ at reflection from a pressure-release surface).

Immediately below we will consider two major areas where traditional ray theory has been found wanting, and recently improved: approaches towards the summation of the rays; and the breakdown of the ansatz, equation (5), in the vicinity of the ray envelope or caustic.

1. Multi-Path Summation

While in principle there are an infinite number of ray paths connecting the source with each observation point in a bounded medium, the total field is generally dominated by less than ten paths. The ray theoretic-solution requires the fully coherent or phased sum of these paths according to equation (5).

a. Long-Range Surface-Image Interference

Until recently, however, computations based upon ray theory assumed an incoherent or rms sum of paths - i.e., the ray intensities were summed without phase. In part, the justification for this procedure was that a range-smoothed transmission-loss curve was desired and it was hoped that the incoherent sum represented a range average. It was also postulated that uncertainties in geometry and the medium precluded sufficiently accurate phase computations to justify a coherent summation. For high frequencies (several hundred hertz) and many geometries, these were reasonable assumptions.

However at low frequencies (less than 100 Hertz) it was found that measured and incoherently computed values of transmission loss differed markedly for shallow sources. This should not be surprising since near the surface the pressure should approach zero, yet the individual ray amplitudes will remain finite. What happens, of course, is that the rays divide into pairs whose components differ only by a surface reflection (Figure 1a). In the approximation of local plane waves the phase difference can be seen (Figure 1b) to be [2]

$$k\Delta\phi = 2kz\sin\theta - \pi \quad . \tag{12}$$

This result was recently generalized by Pedersen to include refraction (Figure 1c) to [3]

$$k\Delta\phi = 2kc_o \int_{\zeta=0}^{z} \frac{\sin\theta(\zeta)}{c(\zeta)}\, d\zeta - \pi \quad . \tag{13}$$

Clearly for shallow-angle rays to sources at low frequencies, $k\Delta\phi \to -\pi$ in either expression and the up- and down-going rays destructively interfere.

The coherent combination of these pairs of paths followed by the incoherent summation of the resulting intensities represents a much better range average than the totally incoherent sum. The phase difference between the paths within a pair is predictable, preserved over significant range intervals, and easily computable from the local geometry without requiring the computation of travel time along the entire ray trajectory. This "semi-coherent" summation has been incorporated in the FACT propagation loss model [4] (along with the incoherent and fully coherent sums), and results based upon the three summations are illustrated for a typical shallow-source/shallow-receiver geometry in Figure 2.

b. Multi-Path "Fluctuations"

As a source or receiver transits the complicated multi-path interference patterns (such as the coherent curve in Figure 2) the signal level fluctuates significantly in time.

The intensity at the field point $\underline{x}$ is given by

$$I(\underline{x}) = \sum_j I_j + 2 \cdot \sum_j \sum_{m<j} (I_j \cdot I_m)^{1/2} \cos(k(\phi_j - \phi_m)), \qquad (14)$$

where I_j are the ray intensities at $\underline{x}$. Assuming that the paths near $\underline{x}$ may be represented by locally plane waves, the phase difference between paths at range $x+\Delta x$ may be obtained from that at x:

$$k(\phi_j - \phi_m) = k(\phi_j(x) - \phi_m(x)) + k\Delta x(\cos\theta_j - \cos\theta_m). \qquad (15)$$

Hence the spectrum of signal fluctuations in range (Δx) will exhibit certain periodicities governed by the cosines of the angles of the interfering paths with powers proportional to the products of their intensities. Similarly if perturbations in the medium alter the phases at $\underline{x}$ with time, the signal also fluctuates. Such temporal multipath fluctuations are significantly larger in amplitude than any individual focusing or defocusing effects produced by the medium.

2. Caustics

The second major area in which the traditional approach to ray acoustics must be augmented is the evaluation of the acoustic field in the vicinity of a caustic. As depicted in Figure 3a, a caustic corresponds to the envelope of a family of rays. On the caustic the field amplitude as predicted by equation (6a) is infinite, since the cross-section of the

ray tube converges to zero. On the shadow-zone side the classical field is zero since, in this region no rays exist. In the limit as $k \to \infty$ this is a reasonable description, however at lower frequencies, the field transits smoothly from the illuminated region (in which real rays exist) to the diffraction region where the field exponentially decays and no 'real' rays exist. In fact, as the frequency decreases the diffraction increases to the extent that large regions exist where it can no longer be ignored.

The solution to this problem has been to employ an asymptotic evaluation of the continuous representation of equation (8) involving either the method of steepest decents or the method of stationary phase, under the assumption that the integrand does not contain any singularities close to the points of stationary phase.

a. Smooth Caustics

The simplest caustic system evolves from two rays arriving at each observation point $\underline{x}$ within the illuminated region. As the caustic is approached the two stationary-phase points in equation (8) coalesce as do the two rays in the illuminated region. The field at the caustic may then be found by proper evaluation of equation (8) at this limit and involves $f_{\xi\xi\xi}$ (see Brekhovskik[5]). However, in order to use this field in the context of the traditional ray approach, it is necessary to provide a means for smoothly

connecting the field at the caustic to the diverging field in the illuminated region.

In this respect, Kravtsov[6] and Ludwig[7] independently developed a uniform asymptotic evaluation of the field valid on and near the caustic as a function of the geometrical acoustic phases ϕ_1, ϕ_2 and amplitudes A_1, A_2 of the two rays (Figure 3b) passing through each point in the illuminated region[6]:

$$P \sim \pi^{1/2} \cdot e^{ik(\phi_2+\phi_1)/2} \cdot e^{-i\pi/4} \cdot \left[u^{1/4}(A_2+A_1)\mathrm{Ai}(-u)+iu^{-1/4}(A_2-A_1)\mathrm{Ai}'(-u)\right]. \quad (16a)$$

In equation (16a), Ai and Ai′ are the Airy function and its first derivative with respect to the argument, where u is given by

$$u=\left[\frac{3}{4}\,k(\phi_2-\phi_1)\right]^{2/3} . \quad (16b)$$

In turn, Holford and Spofford[8] have used this result to obtain a non-uniform expression based upon the difference in the caustic and ray curvatures, κ, and the number of rays tangent to the caustic per unit distance along the caustic, $\frac{d\theta}{dL}$,

$$P \sim \left(\frac{\cos\theta'}{x}\right)^{1/2}\left[\left(4\pi\frac{d\theta}{dL}\right)^{1/2} e^{i(k\phi_c - \pi/4)}\right.$$

$$\left.\cdot\left(\frac{k}{2n^2|\kappa|}\right)^{1/6} \mathrm{Ai}\left(-(2n^2k^2|\kappa|)^{1/3}\Delta z\right)\right], \qquad (17)$$

where Δz in the distance measured normal to the caustic surface.

The Kravtsov-Ludwig result is "uniform" in the sense that while the coefficients of the Ai and Ai′ terms require the rays for their evaluation, they may be analytically continued from the illuminated region into the shadow zone where there are no rays. The Holford-Spofford result corresponds to the linear term in this analytic continuation and is defined for Δz both positive (illuminated region) and negative (shadow zone).

b. Cusped Caustics and Four-Ray Systems

Just as the geometrical-acoustics amplitude is invalid at smooth caustics where $f_{\xi\xi}=0$, the smooth-caustic expressions are not valid when $f_{\xi\xi\xi}=0$. In two-dimensional ray pictures the first situation occurs along caustic curves and the second occurs at points where two caustics are cotangent as shown in Figure 4a. Note that inside the cusp, C, there are three rays through each point vice the two-rays in the illuminated region of a smooth caustic. The nonuniform expression for the field near these cusped caustics was obtained by Pearcey[9] and is described in some detail in Brekhovskikh[10]. Whereas for smooth caustics the uniform field is given in

terms of two quantities κ and $\frac{d\theta}{dL}$, the cusped caustic field is governed by the single parameter β, where

$$P \sim \pi^{-1/2} e^{i(k\phi_c - \pi/4)} (nk\beta)^{1/4} \left(\frac{\cos\theta'}{x}\right)^{1/2} \cdot Pe\left\{\left[(nk)^3\beta\right]^{1/4} X', -\left[nk\beta\right]^{1/2} Y'\right\} , \qquad (18)$$

X' and Y' are cusp-centered coordinates with the Y' coordinate the axis of the cusp, and

$$\left(\frac{X'}{2}\right)^2 = \beta\left(\frac{Y'}{3}\right)^3 , \qquad (19)$$

the equation of the cusp. $Pe(x,y)$ is the Pearcey Function and is discussed in detail in Reference [1], and $k\phi_c$ is the geometrical-acoustics phase at the cusp.

Ludwig's general results have been applied to the cusped caustic yielding a result similar to Equation (18) for the uniform field near a cusped caustic in terms of the geometrical amplitudes and phases of the three rays associated with the cusp. Approaching the cusp along either smooth caustic, both smooth-caustic parameters, κ and $\frac{d\theta}{dL}$ become infinite. The rate at which they approach infinity determines β:

$$\beta = \sqrt[6]{\left(\frac{d^2L}{d\theta^2}\right)_{cusp}} . \qquad (20)$$

While β is in general quite difficult to calculate, it does simplify considerably in the case where the axis of the cusp is horizontal. As it so happens, this case becomes of extreme importance in range-independent media (i.e., $c(\underline{x})=c(z)$) since a horizontal cusp will form at the same depth as the source.

While higher order singularities are possible, the most complicated ray geometry typically encountered is when a smooth caustic is quite close to a cusp as shown in Figure 4b. In this case the two fields may no longer be treated as distinct and a basic four-ray system is generated where it is possible that even the smooth- and cusped-caustic expressions may break down. For most cases of interest, however, a phased sum of the two distinct fields has been found to be adequate.

3. False Caustics

One of the major concerns in using ray acoustics has been the functional representation for the sound-speed profile since it governs the ease with which rays may be traced and intensities computed. Pedersen[11] and others have shown that when a sound-speed profile with continuous derivatives is approximated by linear segments, there exists the possibility of introducing false or extraneous caustics. The actual problem, on the other hand, does not lie with the profile representation but instead with the traditional

approach to ray acoustics. The results of the modified ray theory [12] (MRT) developed by Murphy and Davis graphically illustrate this point.

MRT is based upon a generalized Wentzel-Kramers-Brillouin (WKB) expansion of equation (8) and, as such, includes the caustic modifications mentioned above. Murphy and Davis have shown that this procedure leads to a frequency-dependent displacement of the ordinary ray-theory ranges. Employing the simple profile depicted in figure 5 , ordinary ray theory would predict the formation of a caustic due entirely to the discontinuity in the gradients of the profile at the juncture of the two segments. The ray tangent to the caustic coincides with the minimum ($\frac{\partial x}{\partial \theta} = 0$) in range on the accompaning angle (θ)- vs. range (x) plot. The MRT angle-vs.-range plot for the same case is also shown. At a high frequency MRT still shows a caustic (in fact, two: one associated with the minimum in range, and another associated with the smooth maximum in range). However, as the frequency is decreased the angle-vs.-range curve is completely smoothed out and the caustic of ordinary ray theory disappears.

A more complicated example (figure 6) was recently provided by Weinberg [13], using three different realizations of an Epstein profile: piecewise linear, piecewise quadratic, and cubic spline. In all three forms, the

source was placed on the axis of the Epstein profile with the depth of the observation point situated somewhat shallower. The results at a frequency of 1 kHz. are also based upon a generalized WKB expansion of equation (8). Even at 1 kHz., all three representations provide essentially the same results. Thus, with a proper analysis of the caustic fields, the profile representation is not critical to the total field.

This type of insight into the frequency-dependent smoothing of the $x(\theta)$ curve lead directly to the development of the FACT model,[4] where the primary concern was not only with speed of computation, but also being able to provide meaningful asymptotic caustic values along with the effects of coherence. Representing the profile in terms of linear segments permitted a rapid trace of the rays but also introduced the possibility of false caustics as discussed above. By limiting the angle-vs.-range curve behavior for a particular ray family to two-degrees of freedom (i.e., using a quadratic fit) and also by carefully selecting the rays to be traced with respect to the profile, the problem of false caustics was reduced significantly.

In range-dependent media the profile representation takes on a different aspect, for the primary difficulty here is not in tracing rays, but in defining how the medium will vary between specified profiles.

Two methods for connecting the profiles are in common use. The first method[14] allows the sound-speed representation to be arbitrary in depth but linear, quadratic, or cubic in range at fixed depth. The second method[15] is based upon segmenting the region between the profiles into triangular sectors where two vertices of the triangle correspond to two points on one of the profiles and the third vertex corresponds to a point on the other profile. Along the connecting legs of the triangle the sound-speed varies as $c(z,x)=c_o+az+bx$. Both methods have their drawbacks. The first method is easy to automate but leads to ray-tracing difficulties since closed form expressions for the ray paths are not available. Additionally, this method can lead to totally unreasonable profiles at intermediate ranges between reasonable specified profiles. The second method is quite difficult to automate in that it usually requires an oceanographer to determine the required connections. Aside from this problem, however, the linearity of the sound speed leads to a closed form expression for a ray's path within each triangular sector enabling a relatively rapid trace.

4. Summary of Ray Acoustics

With the advances in classical ray theory described above, ray acoustics can and has been successfully extended

down to frequencies on the order of 25 Hz. The primary difficulty with these modifications lies in their complete automation. In many cases, especially for range-dependent media, the ray pathologies may be so complex as to require a hand analysis.

B. Normal Modes

Normal-mode theory in underwater acoustics is based upon the initial requirement that the sound speed vary as a function of depth only, i.e., $c(\underline{x})=c(z)$. This simplification permits the reduction of the wave equation by separation of variables, leading to a system of two linear differential equations, one for the depth dependence of the field, the other for the range dependence. The total field $P(\underline{x})$ is then given by the product of the two separable solutions integrated over the separation parameter, λ. Specifically, the result may be represented by a Bessel-Hankel transform[16],

$$P(\underline{x})=\int_{\lambda=0}^{\infty} \hat{P}(z,z',\lambda)J_o(\lambda x)\lambda d\lambda, \qquad (21)$$

where J_o is the zeroth order Bessel function, and the depth function $\hat{P}$ satisfies

$$\left[\frac{d^2}{dz^2}+(k^2n^2(z)-\lambda^2)\right]\hat{P}(z,z',\lambda)=-\frac{1}{2\pi}\delta(z-z'), \qquad (22)$$

λ is the radial wave number and may be assumed to be complex.

By modifying the integration contour an alternative to the continuous standing-wave representation of equation (21) can be derived,

$$P(\underline{x}) = \frac{1}{2}\int_{\infty e^{i\pi}}^{\infty} \hat{P}(z,z',\lambda) H_o^{(1)}(\lambda x)\, \lambda d\lambda, \qquad (23)$$

such that the zeroth-order Hankel function of the first kind, $H_o^{(1)}$, now represents an outgoing wave under the time-dependence $e^{-i\omega t}$. Equation (23) can be numerically integrated as DiNapoli has done in his Fast Field Program (FFP). In the FFP, the integral is cast into the form of a Fast Fourier Transform by employing the asymptotic form of the Hankel function. This procedure, coupled with a judicious selection of the functional form of the sound-speed profile to permit the rapid calculation of the constituents of $\hat{P}$, allows a practical evaluation of equation (23).

With respect to the normal mode expansion, the bulk of the remaining problems center about the evaluation of the depth function $\hat{P}(z,z',\lambda)$. All of these methods are subject to the boundary constraints of a pressure-release surface, Sommerfield's radiation condition, and continuity conditions at discontinuities in both the water column and bottom. Additionally, the particular form of the solution

$\hat{P}(z,z',\lambda)$ depends upon the functional description of the sound speed-profile itself.

The general normal-mode expansion may be obtained by identifying the singularities of $\hat{P}(z,z',\lambda)$ and subsequently deforming the integration contour about the singularities. Depending upon how the sound-speed profile is terminated, three classes of singularities are evident: (1) a finite number of poles along the real λ axis (assuming the medium is lossless), (2) an infinite number of complex poles, and (3) branch points which appear pairwise. For sound-speed profiles encountered in underwater acoustics, the branch-point singularities are ordinarily associated with the modeling of the ocean bottom.

In order to illustrate the physical significance of these mathematical singularities consider a sound-speed profile terminated by an isovelocity halfspace ($c(z>z_B)=c_H$) such as that illustrated in figure 7. Restricting attention to the first quadrant ($Re(\lambda)>0, Im(\lambda)>0$) of the complex λ plane, the isovelocity termination will lead to a branch point singularity at $\lambda=\lambda_H=\frac{\omega}{c_H}$ and the water column will produce a finite number of poles λ_m along the real λ axis such that $\lambda_H<\lambda_m<\lambda_{max}=\frac{\omega}{c_{min}}$. In a rather loose sense, contributions to the field from the poles along the real axis correspond to axial rays, for λ_m close to λ_{max} and

bottom-reflected rays for $\lambda_m \simeq \lambda_H$. The influence of the infinity of poles off the real-λ axis to the field depends on the choice of branch cut.

Most normal mode programs today are based upon the Pekeris-type branch cut[17] illustrated in figure 7 . The corresponding integration contour leads to a symbolic representation for equation (23) as

$$2\pi i \sum_{m=1}^{N} (\text{residues for } \lambda_m \ni : \mathrm{Im}(\lambda_m)=0) \qquad (24)$$

$$+ 2\pi i \sum_{m=N+1}^{\infty} (\text{residues for } \lambda_m \ni : \mathrm{Re}(\lambda_m), \mathrm{Im}(\lambda_m)=0)$$

$$+ \int (\text{Perkeris Branch Cut}) + \int (\text{Semi-Circle}, \ |\lambda| \sim \infty).$$

An alternative representation is obtained by employing the Ewing-Jardetsky-Press (EJP) branch cut (figure 7),

$$2\pi i \sum_{m=1}^{N} (\text{residues for } \lambda_m \ni : \mathrm{Im}(\lambda_m)=0) \qquad (25)$$

$$+ \int (\text{EJP Branch Cut}) + \int (\text{Semi-Circle}, |\lambda| \sim \infty),$$

where the integration at infinity along the semi-circle can be shown to be zero for all cases of interest. Labianca[16] has pointed out that the Pekeris cut has practical as well as theoretical problems, particularly since the residue sum

diverges for ranges less than $\sqrt{3}\cdot(z+z')$. For ranges greater than this the residue sum converges and the two representations are equivalent.

Representing the EJP branch cut in equation (25) as a finite integration on the real-λ axis and an infinite integration along the complex-λ axis, the normal mode solution can be explicitly expressed as

$$P(\underline{x}) = \sum_{m=1}^{N} C_m(\lambda_m)\hat{P}_m(z,\lambda_m)\hat{P}_m(z',\lambda_m)H_o^{(1)}(\lambda_m x) \qquad (26)$$

$$+\int_{\lambda_R=0}^{\lambda_{R_{min}}} f(\lambda_R,z,z,x)\,d\lambda_R + \int_{\lambda_c=0}^{\infty} g(\lambda_c,z,z',x)\,d\lambda_c,$$

where the so-called eigenfunctions $\hat{P}_m$ and eigenvalues λ_m satisfy the discretized form of equation (22):

$$\left[\frac{d^2}{dz} + (k^2n^2(z)-\lambda_m^2)\right]\hat{P}_m = -\frac{1}{2\pi}\delta(z-z') \qquad (27)$$

and the particular boundary conditions, and where the $C_m(\lambda_m)$ are the mode-amplitude weighting factors as determined by normalizing the eigenfunctions. Thus the normal-mode expansion consists of a classical sum of modes plus a continuum of modes which arise from the EJP branch cut. This continuous spectrum has frequently been ignored as a result of the more common usage of the Pekeris representation (equation (24)).

Considerable effort in a normal-mode solution is consumed finding the singularities of the integrand within equation (21). One such method involves guessing λ_m, integrating the differential equation (27) to one of the boundaries (usually the surface) and iterating on λ_m until the boundary condition is satisfied within prescribed tolerances. Such tolerances do not guarantee overall accuracy, and control remains a persistent problem. Also since the number of modes and the number of iterations per mode are roughly proportional to frequency, normal-mode solutions are practical only for low frequencies. However they do represent the exact control solution against which all others may be tested. These tests then allow the extension of more general techniques to the range-dependent environment with some confidence.

Some extensions of the normal-mode solutions to range-varying media (i.e., $n(\underline{x})=n(x,z)$ have been attempted. These generally fall into one of three approaches:

(i) Those which assume no cross-coupling between modes;

(ii) Those which assume at least weak coupling between modes at different range intervals;

(iii) Those which require matching a boundary condition for the total field at some x for all z.

The adiabatic approach of (i) requires that all energy propagating in mode number 'n' remain in the mode independent of range[22, 26]. The phase velocity (implicit in λ_m), then, varies with range as new sound-speed profiles are introduced. The weak-coupling approach of (ii) requires a large number of mode computations at different ranges to evaluate the weakest form of coupling between each mode and only its immediate neighbors. The third approach, (see Kanabis[18]) requires continuity of pressure across an interface at arbitrary range. The field at the interface is computed in terms of the modes just prior to the interface, and then decomposed into the new modes defined by the profile just after the interface. This procedure neglects any backscatter and requires either a large number of mode calculations, or places rather stringent requirements on the range variation.

C. Parabolic Equation

The final approach to be considered here is the parabolic-equation technique, where the solution to the elliptic wave equation, equation (1), is initially assumed to be of the form

$$P(\underline{x}) = \psi(x,z)H_o^{(1)}(kx). \qquad (28)$$

The Hankel function, $H_o^{(1)}(kx)$, represents the primary radial

dependence of the field in terms of an outward propagating cylindrical wave.

To this point the only approximation made is the assumption of cylindrical symmetry. The second approximation is that the observation point, x, is many wave lengths from the source (i.e., kx>>1). Subsequently the asymptotic form of the Hankel function may be used to obtain from equation (28)

$$\psi_{xx}+2ik\psi_x+\psi_{zz}+\psi k^2(n^2-1) = 0 \qquad (29)$$

plus terms of order ψ/kx^2. Finally, employing the approximation

$$\psi_{xx}<<2ik\psi_x \ , \qquad (30)$$

which neglects backscatter and is generally described as valid only for components of the field propagating at small angles with respect to the horizontal, the parabolic equation of Leontovich[19] and Fock[20] is derived:

$$i\psi_x+\frac{1}{2k}\psi_{zz}+\frac{k}{2}(n^2-1)\psi = 0 \qquad (31)$$

Although the parabolic approximation has been available for some time, only recently have efficient integration

schemes been applied to it, namely, the introduction by Tappert and Hardin[21] of the split-step Fast Fourier Transform numerical integration algorithm. This algorithm marches the solution away from the source on an equi-spaced depth grid. The value of ψ at a new range $x+\Delta x$ is obtained from the solution at sept x by

$$\psi(x+\Delta x,z)=e^{i\Delta x k(n^2-1)/2}\mathcal{F}^{-1}\left[e^{-i\Delta x \ell^2/2k}\mathcal{F}(\psi(x,z))\right], \quad (32)$$

where $\mathcal{F}$ is the Fourier transform, $\mathcal{F}^{-1}$ its inverse, and ℓ the transform variable. This technique is easily implemented, highly efficient, and even in the above form, sufficiently accurate for most applications.

The parabolic approximation, as expressed by the inequality in equation (30), has been shown to result in an error in the phase velocity of the normal modes in layered media[22]. The phase velocity error, in turn, can cause substantial shifts in the range of the caustic regions. Recently Brock, Buchal, and Spofford[23] have been able to reduce the magnitude of the error by using the PE technique to solve a pseudo-problem where the refractive-index profile, n(z) has been transformed into a new set of points $(\tilde{n},\tilde{z})$. This transformation takes on a particularly simple form for the majority of cases of interest, namely

$$\left.\begin{aligned}\tilde{z}&=zn^{1/2},\\ \tilde{n}&=\sqrt{2n-1}\ .\end{aligned}\right\} \quad (33)$$

Within the accuracy of the WKB approximation, the normal modes for this new environment have the same phase velocities as the equivalent wave-equation modes in the original environment, and the depth transformation preserves the relationship between observation depths and mode turning points.

It would not be an exaggeration to say that the PE has revolutionized propagation modeling by providing a wave solution with full mode coupling for the range-dependent environment. It is easy to implement, efficient, and may be used to map out the full acoustic field in both range and depth. Since both the range step and depth mesh are proportional to the acoustic wavelength, PE, like normal modes, is practical for low frequencies only. Computer codes have been implemented for deepwater studies up to 300 Hz, however, typical applications are limited to approximately 100 Hz.

II. COMPARISON OF TECHNIQUES

In this section we compare frequency-modified ray theory and the PE technique with the exact solution as given by normal-modes. Consequently the examples are limited to the range-independent environment. Additionally, the comparisons which will be made will be for a high-loss bottom concentrating on the refracted and RSR paths only.

Initially we consider a simple pressure-gradient profile for a shallow source (60 feet) at a frequency of 25 Hz and a deep receiver (7200 feet). The results of the three techniques are compared in figure 8 where, specifically, the three models are FACT[4] - a ray model with caustic corrections and surface-image interference; PE without the profile transformation described in Section I-C , and an N-layer normal-mode model developed by Stickler at Penn State Applied Research Laboratory[24]. While Stickler's model can compute contributions from the continuous spectrum, it was run for the discrete modes only. In this geometry a smooth caustic occurs at the receiver depth at approximately 30 nm intervals. The rapid oscillations seen within the caustic regions of both the normal-mode and PE results are due to the two-ray interference. The ray-theory model has intentionally averaged these oscillations, since they do not reflect a change in average level. It has, however,

included the semi-coherent combination of paths which, for this frequency and source depth increase the average transmission loss by approximately 8 dB over the value the incoherent summation would yield. This figure also illustrates the effects of excluding the continuous spectrum in the normal-mode calculations. For ranges less than 8 nm the normal-mode results are seen to depart dramatically from both the ray-theory and PE models, since the energy associated with these high-angle paths is not included in the discrete system.

The second example (figure 9) also is based upon a pressure-gradient profile but now the source is at the same depth as the receiver (7200 feet). In this geometry a horizontal cusp is developed (as illustrated in figure 4a) at 22 nm and repeats with a 22 nm period. A smooth caustic is also present at this depth at 35 nm corresponding to the surface reflection of one of the smooth caustics associated with the first cusp. In this case the smooth- and cusped-caustics are well-separated and the ray-theory results are seen to agree with the results of the other two models.

The final case considered is based upon a typical deep-water sound-speed profile (figure 10) where the source and receiver are situated such that two ray families propagate: a totally refracted (RR) family and a refracted-surface

reflected (RSR) family. Figure 11 initially compares the ray solution with that of normal modes (again at 25 Hz). The agreement is generally excellent even though the ray model does make a clearcut distinction between the RR and RSR caustic regions while the mode model does not. The apparent constructive interference between the RR and RSR caustics is not accounted for in the ray model since these families of rays are combined incoherently. Figures 12 and 13 compare the PE technique with the normal-mode solution for exactly the same case. In figure 12 PE was run without the profile transformation discussed previously, resulting in a displacement of the PE convergence zone relative to the normal-mode result. With the profile transformation PE, figure 13, now accurately matches not only the convergence-zone ranges but much of the CW multipath fine structure.

In the context of range-independent environments it is seen that the three basic techniques have largely converged. Wave-length dependent corrections to ray theory have been developed which permit its extension to much lower frequencies. Many of the limitations of the parabolic equation are now more clearly understood and the most limiting aspects of the small-angle approximation have been overcome. This apparent convergence is not intended to imply that each technique is equally applicable to any problem. In the next section we shall consider the applicability of these techniques to the study of certain classes of oceanographic phenomena.

III. APPLICATIONS TO THE STUDY OF OCEANOGRAPHIC FEATURES

Many of the acoustically interesting oceanographic features correspond to a medium which varies not only as a function of range and depth but also azimuth and time. In the deterministic techniques discussed above the environment is frozen in time and generally treated as azimuthally symmetric. The effect of transverse gradients and out-of-plane reflection can be important in some cases, however a number of significant oceanographic features can be analyzed without including these effects and without any loss of generality.

Normal-mode techniques are by far the most limited since they cannot accommodate rapid variations in range. Instead, they can be used within the context of perturbation theory to study the acoustic effects of small inhomgeneities superimposed on a basically range-independent profile. Perturbation theory has also been applied successfully by Labianca and Harper[25] to assess the influence of surface roughness on low-frequency propagation. Only the largest scale oceanographic features such as the gradual migration of the sound-channel axis towards the surface in the North Pacific can be legitimately analyzed within the adiabatic approximation[26]. Macro-scale features such as fronts and eddies are too abrupt for the adiabatic technique[27] while probably too gradual for the abrupt transition approaches of Kanabis, et al.

Ray theory, in principle, is the most powerful since it can accomodate rapid variations with refraction through large angles. In studying small perturbations, enough rays must be considered to adequately illuminate all features of interest, and, if necessary, detailed caustic calculations may be required to assess the true influence of these features on the acoustic phase and amplitude. For larger scale oceanographic features ray techniques are most useful for illustrating quatitative effects and are especially illuminating when used in conjunction with field-mapping computations such as PE.

PE is by far the most versatile technique, though of course, limited to low frequencies and shallow angles. Fortunately the propagation paths of interest in analyzing oceanographic features are sufficiently shallow to be accurately treated, and the features themselves are not expected to produce sufficient backscatter to violate the parabolic approximation[28].

In studying bottom-reflectivity questions, normal modes are most appropriate since they can accomodate both discontinuities (which PE using the split-step FFT cannot), and partial reflections (which ray theory typically does not). Additionally normal mode programs[29] have been extended to include shear waves in the bottom.

IV. SUMMARY

Concurrent advances in the application of normal-mode and ray theory to ocean acoustics, coupled with the introduction and refinement of the parabolic-equation technique, have brought what were previously considered divergent and non-intersecting approaches into agreement over a substantial common ground of applications. The demonstrated success of these techniques in the study of deterministic phenomena portends their fruitful application in the stochastic domain. While each approach has its unique strengths and weaknesses, their combined power should be sufficient to attack a large number of previously impenetrable questions.

REFERENCES

1. R. L. Holford, Continuation of LRAPP (CONFIDENTIAL), Reference 7, "Modifications to Ray Theory Near Cusped Caustics" (Unclassified), February (1972), Bell Laboratories on Contract N00014-69-C-0088, p. 5.

2. F. E. DeAngelis and C. W. Spofford, "Surface Image Interference Effects in Long-Range Active Sonar Systems" (U), 20 February (1970), Bell Laboratories on Contract N00014-69-C-0074 (SECRET).

3. M. A. Pedersen, D. F. Gordon, and D. White, "Surface Decoupling Effects," unpublished tech. memo to Long Range Acoustic Propagation Project (LRAPP).

4. C. W. Spofford, "The FACT Model", Vol. 1, Maury Center Report 109, November (1974).

5. L. M. Brekhovskikh, Waves in Layered Media, Academia Press, New York, (1960), p. 484.

6. Yu. A. Kravtsov, "One Modification of the Geometrical Optics Method," Soviet Radiophysics, Vol. 7, (1964), pp. 104-117.

7. D. Ludwig, "Uniform Asymptotic Expansions at a Caustic," Commun. Pure Appl. Math, Vol. 19 (1966), pp. 215-250.

8. C. W. Spofford and R. L. Holford, "Calculation of the Field near a Smooth Caustic by means of Uniform and Nonuniform Asymptotic Approximations Derived from Ray Theory", (to be published).

9. T. Pearcey, "The Structure of an Electromagnetic Field in the Neighborhood of a Cusp of a Caustic", Philos. Mag., Vol. 37 (1946), pp. 311-317.

10. L. M. Brekhovskikh, pp. 492-296.

11. M. A. Pedersen, "Acoustic Intensity Anomalies Introduced by Constant Velocity Gradients," Journal of the Acoustical Society of America (JASA), Vol. 33 (1961), pp. 465-474.

12. E. L. Murphy and J. A. Davis, "Modified Ray Theory for Bounded Media," JASA, Vol. 56, (1974), pp. 1747-1760.

13. H. Weinberg, "Application of Ray Theory To Acoustic Propagation In Horizontally Stratified Oceans," JASA, Vol. 58 (1975), pp. 97-109.

14. See, for example:
J. J. Cornyn, "Grass: A Digital-Computer Ray-Tracing and Transmission-Loss-Prediction System," Naval Research Laboratory Report 7621, Vol. 1, Washington, D. C., December (1973).

15. C. W. Spofford, "The Future of Long-Range Acoustic Transmission-Loss Prediction," Paper presented at the 28th U.S. Navy Symposium on Underwater Acoustics, Washington, D.C., November (1970).

16. A particularly in-depth discussion of the different representations may be found in:
F. M. Labianca, "Normal Modes, Virtual Modes, and Alternative Representations in the Theory of Surface-duct Sound Propagation," JASA, Vol. 53 (1973), pp. 1137-1147.

17. Both the Pekeris and EJP branch cuts are lucidly discussed in:
D. C. Stickler, "Normal Modes In Ocean Acoustics", Penn. State Univ. Applied Research Laboratory Tech. Memo TM 75-24, State College, Pa., February (1975).

18. W. G. Kanabis, "A Shallow Water Acoustic Model For Ocean Stratified in Range and Depth", Naval Underwater Systems Center (NUSC) Tech. Report 4887-I, New London, Conn., March (1975).

19. M. A. Leontovich and V. A. Fock, J. Phys. of the USSR, Vol. 10 (1946), p. 13.

20. V. A. Fock, J. Phys. of the USSR, Vol. 10 (1946), p. 399.

21. F. D. Tappert and R. H. Hardin, SIAM Review, Vol. 15 (1973), p. 423 (abstract).

22. S. T. McDaniel, "Propagation of Normal Modes in the Parabolic Approximation," JASA, Vol. 57 No. 2, (1975), pp. 307-311.

23. H. Brock, R. Buchal, and C. W. Spoford, "Modifying the Sound-Speed Profile to Improve the Accuracy of the Parabolic Equation Technique," (to be published).

24. D. C. Stickler, "A Normal Mode Program with both Discrete and Branch Line Contributions," JASA, Vol. 57 (1975), pp. 856-861.

25. E. Y. Harper and F. M. Labianca, "Perturbation Theory for Scattering of Sound from a Point Source By a Rough Surface In the Presence of Refraction," JASA, Vol. 57 No. 5, (1975), pp. 1044-1051.

26. R. Graves, A. Nagl, and H. Uberall, "Underwater Sound Propagation Described by Range-dependent Normal Modes," JASA, Vol. 57 Suppl. No. 1, (1975), p. 564. (abstract).

27. D. M. Milder, "Ray and Wave Invariants for SOFAR Channel Propagation," JASA, Vol. 46 No. 5 (Part 2), (1969), pp. 1259-1263.

28. H. P. Bucker, "Sound Propagation Calculations Using Bottom Reflection Functions," Physics of Sound In Marine Sediments edited by L. Hampton, Plenum Press, New York, pp. 223-239, (1974).

29. H. W. Kutschale, "The Integral Solution of the Sound Field in a Multilayered Liquid-Solid Half Space with Numerical Computations for Low-Frequency Propagation in the Artic Ocean," Lamont-Doherty Geological Observ. Tech. Report CU1-70.

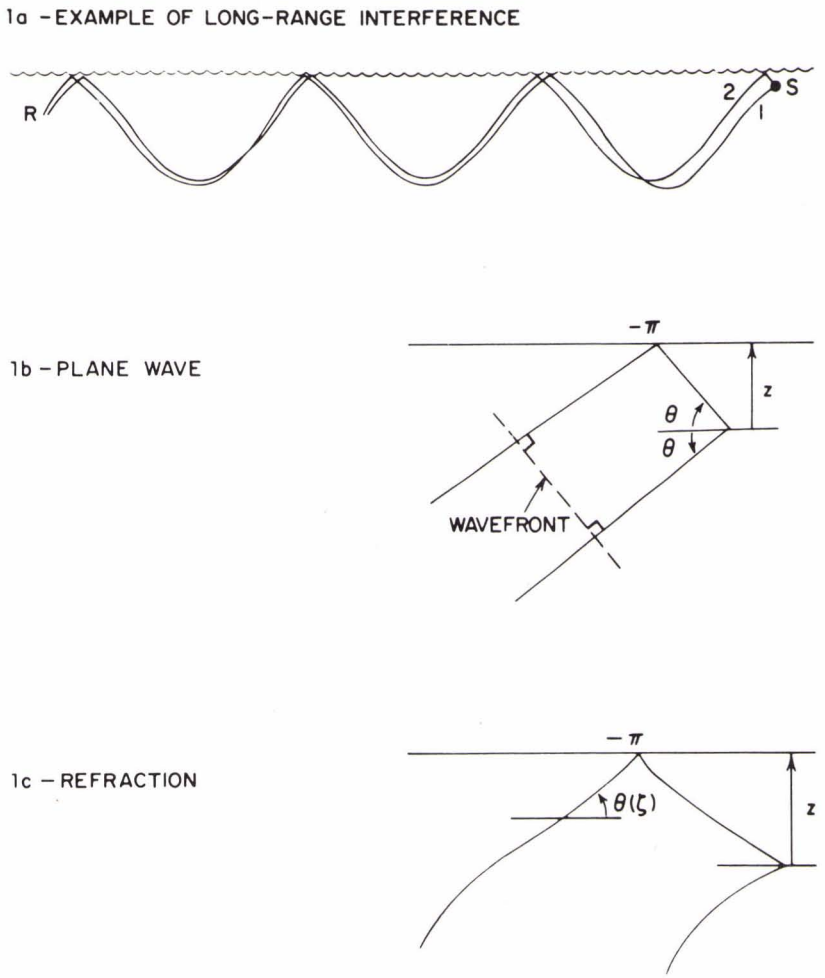

FIG. 1 SURFACE IMAGE INTERFERENCE

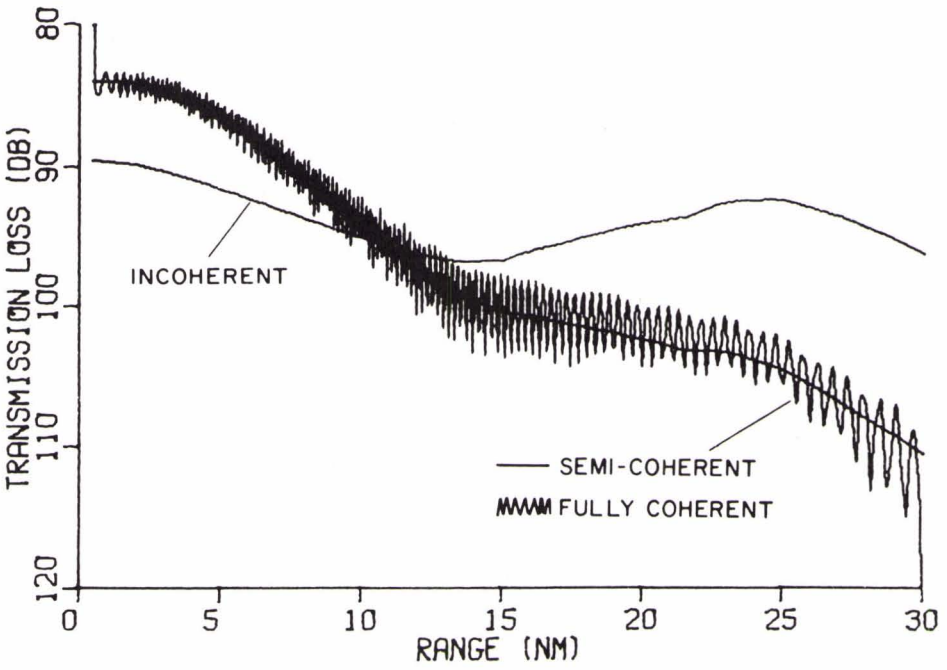

FIG. 2 FACT COMPARISON OF INCOHERENT, SEMI-COHERENT, AND FULLY COHERENT SUMMATIONS

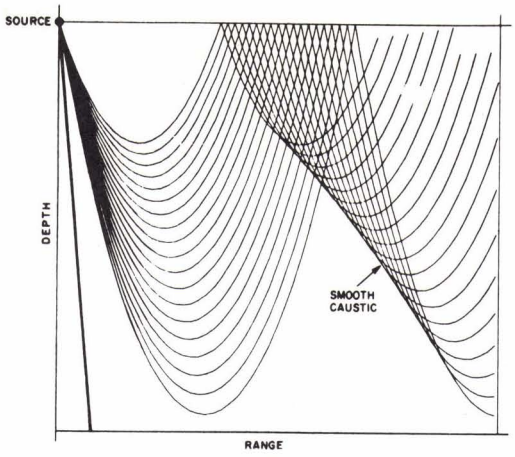

FIG. 3a
DEVELOPMENT OF A SMOOTH CAUSTIC

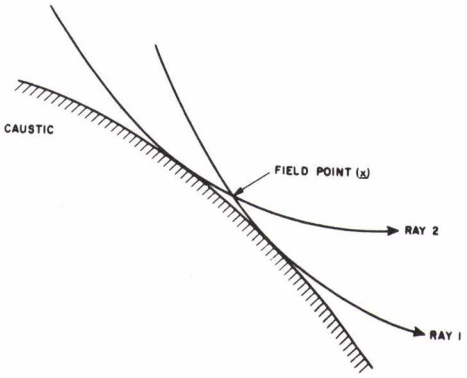

FIG. 3b
RAYS DEFINING FIELD NEAR A CAUSTIC

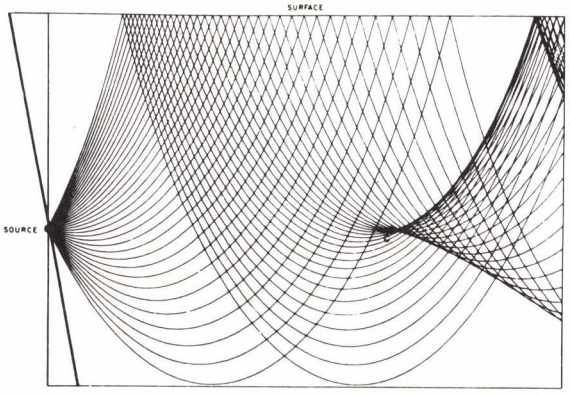

FIG. 4a
DEVELOPMENT OF A CUSPED CAUSTIC

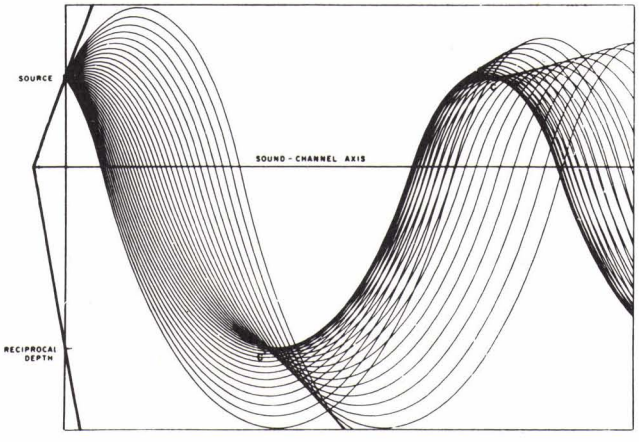

FIG. 4b
DEVELOPMENT OF A FOUR-RAY SYSTEM
(SMOOTH PLUS CUSPED CAUSTIC)

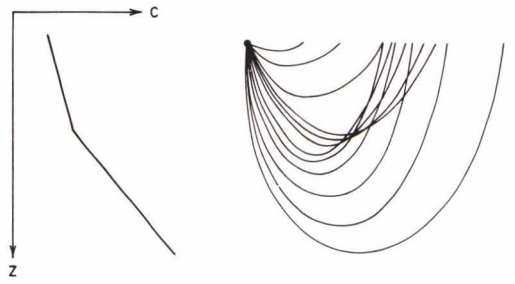

FIG. 5
GENERATION OF A FALSE CAUSTIC

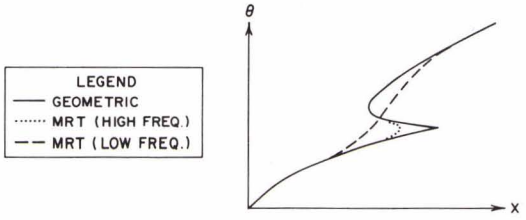

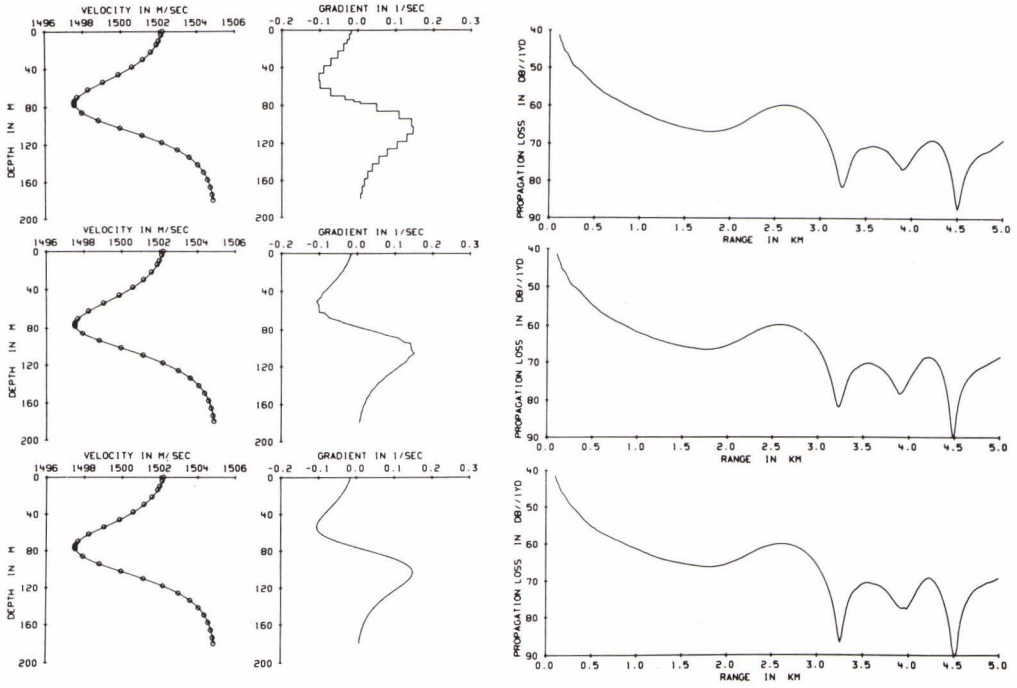

FIG. 6 THREE REPRESENTATIONS FOR AN EPSTEIN PROFILE (AFTER WEINBERG)

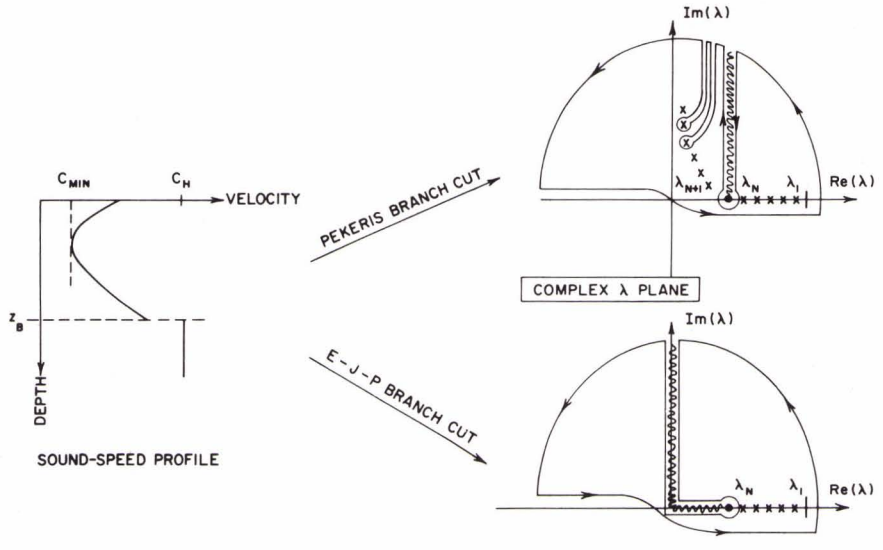

FIG. 7
TWO INTEGRATION CONTOURS DEFINING THE NORMAL MODE EXPANSION